Controllable Single Cooper Pair Splitting in Hybrid Quantum Dot Systems

de Jong, Damaz; Prosko, Christian G.; Han, Lin; Malinowski, Filip K.; Liu, Yu; Kouwenhoven, Leo P.; Pfaff, Wolfgang

Important note
To cite this publication, please use the final published version (if applicable).
Please check the document version above.

Editors' Suggestion

Controllable Single Cooper Pair Splitting in Hybrid Quantum Dot Systems

Damaz de Jong[,1] Christian G. Prosko[,1,*] Lin Han,[1] Filip K. Malinowski[,1]
Yu Liu[,2] Leo P. Kouwenhoven,[1] and Wolfgang Pfaff[3]

[1]*QuTech and Kavli Institute of Nanoscience, Delft University of Technology, 2600 GA Delft, Netherlands*
[2]*Center for Quantum Devices, Niels Bohr Institute, University of Copenhagen, Copenhagen, Denmark*
[3]*Department of Physics and Frederick Seitz Materials Research Laboratory,*
University of Illinois at Urbana-Champaign, Urbana, Illinois 61801, USA

Cooper pair splitters hold utility as a platform for investigating the entanglement of electrons in Cooper pairs, but probing splitters with voltage-biased Ohmic contacts prevents the retention of electrons from split pairs since they can escape to the drain reservoirs. We report the ability to controllably split and retain single Cooper pairs in a multi-quantum-dot device isolated from lead reservoirs, and separately demonstrate a technique for detecting the electrons emerging from a split pair. First, we identify a coherent Cooper pair splitting charge transition using dispersive gate sensing at GHz frequencies. Second, we utilize a double quantum dot as an electron parity sensor to detect parity changes resulting from electrons emerging from a superconducting island.

Cooper pairs—bound electron pairs of correlated spin and momentum—are foundational to superconductivity. Interestingly, coherently splitting a Cooper pair produces two entangled electrons forming a Bell state [1]. It is possible to force a pair to split using Coulomb repulsion in a pair of quantum dots (QDs) [2]. Accordingly, Cooper pair splitting (CPS) has been demonstrated in various material systems [3–13], and the resulting electrons' spin was probed through current correlation measurements exploiting spin-polarized QDs [13,14]. In order to confirm and utilize entanglement of the electrons from a split pair, however, it is important to retain them, for example, by removing drain contacts from the QDs. In this manner, retention of electrons from split Cooper pairs was observed using charge sensing of metallic islands [15], though splitting occurred stochastically at sub-Hz rates. Dispersive gate sensing (DGS) provides distinct information from charge sensing, since it is sensitive to the hybridization between charge states [16–30], including between states with a split or recombined Cooper pair.

Probed with DGS, we present the coherent splitting of a single Cooper pair by varying voltages on a device's gate electrodes. Separately, we demonstrate the detection of an unpaired electron emerging from a superconducting island (SCI). This is accomplished within a hybrid system comprising a SCI with normal QDs on either side, decoupled from leads. Multiplexed DGS of resonators coupled to the device's gate electrodes allows us to distinguish charge transitions in the system, and thus label relative charge states. Strikingly, one transition corresponds to two charges from the SCI being loaded into neighboring QDs, imparting a 1 MHz frequency shift on the probed

few-GHz frequency resonator. This transition likely corresponds to CPS arising due to crossed Andreev reflection (CAR), supported by fitting the DGS signal across the transition to an input-output theory model for an effective low-energy Hamiltonian. Next, we show how DGS detects changes in the charge parity of a double quantum dot (DQD) system. Consequently, DGS can replace charge sensing in our CPS scheme while retaining electrons tunneling to the DQD, since no external charge reservoirs couple to the system. Combined with spin manipulation and readout techniques [31,32], these demonstrated capabilities could be used to perform a Bell test on electrons constituting Cooper pairs [33–36].

The devices measured (labeled A and B), shown in Figs. 1(a) and 1(b), consist of an InAs nanowire with an epitaxial Al shell. For both devices, lithographically patterned gates define five QDs in the wire, though the Al covers only the centermost QD (labeled M) such that only this QD has a superconducting pairing interaction. The semiconducting QDs (labeled L, R, and P) have a length of 0.44 μm in both devices, while island M has a length of 1.2 and 0.44 μm in devices A and B, respectively. Every QD is capacitively coupled via top gates to a coplanar waveguide resonator with a common feedline for multiplexed DGS of each QD [28,37–39], depicted in Fig. 1(c). Separate gates control the QDs' chemical potentials and tunnel barriers. For additional fabrication details, see Ref. [28]. We infer the charging energy of the semiconducting QDs from Coulomb diamond measurements to be $E_C^N \approx 250$ μeV (Supplemental Material [40], Sec. SII). From the charge stability diagrams (CSDs) shown in Fig. 1(f), we extract the charging energy of the SCI for device A $E_C^S \approx 100$ μeV and
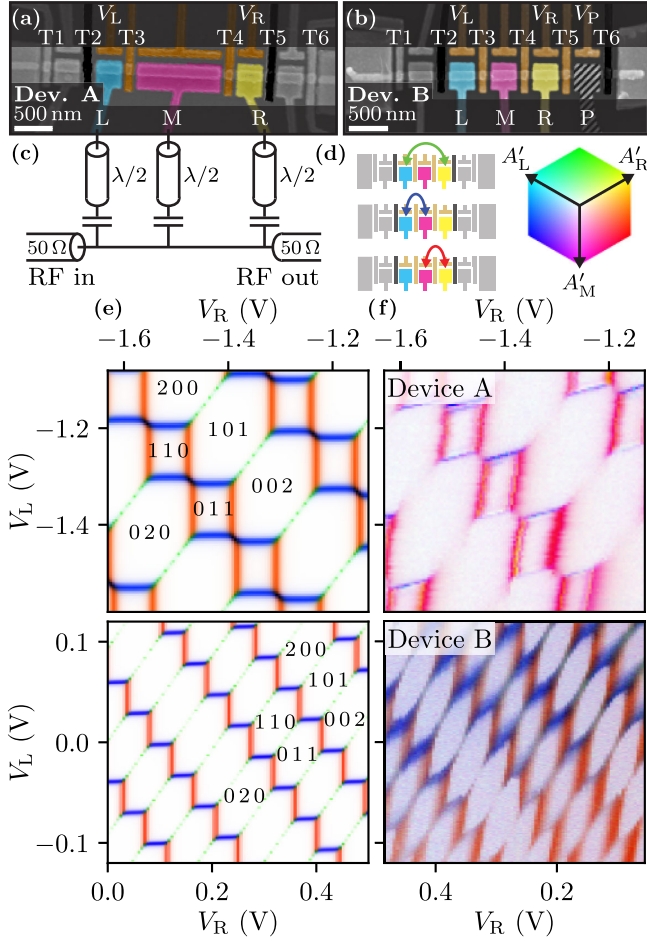
FIG. 1.   Experimental setup and CSDs in the floating TQD regime. (a),(b) False-colored SEM images of devices nominally identical to those measured. Devices A and B are highlighted in the floating triple and quadruple QD regimes, respectively. Gates are shaded with the assigned colors of their coupled resonators. (c) Schematic of the on-chip resonators. We measure transmission through a feedline capacitively coupled to $\lambda/2$ resonators connected to device gates. (d) Shell of the cubic color map for the resonator responses in (e) and (f). For each pair of responding resonators, the corresponding tunneling process is depicted. (e) Simulated resonator responses using energies given in the main text. (f) Measured CSDs of the floating TQD systems. Individual resonator measurements are shown in Supplemental Material [40] Figs. S1 and S2. The CSDs are labeled with charge ground states up to an even charge offset.

its lowest-energy odd-parity state at zero magnetic field $E_0 \approx 130$ μeV. Similarly, for device B, we obtain $E_C^S \approx 350$ and $E_0 \approx 50$ μeV. The differing values of E_0 signify the presence of distinct subgap states, and are generally dependent on gate voltages. With devices A and B we thus compare the regimes of $E_C^S < E_0$ and $E_C^S > E_0$, respectively, verified by a doubling of charge transitions in device A as the magnetic field is increased (Supplemental Material [40], Fig. S5). The former case exhibits a transition corresponding to splitting a Cooper pair, while

in the latter it is suppressed in favor of single-electron tunneling.

Measurements are conducted in a dilution refrigerator at a base temperature of approximately 20 mK. Low-power signals are amplified by a traveling-wave parametric amplifier [41] and a high-electron-mobility transistor.

We begin by investigating a floating triple quantum dot (TQD) configuration. By measuring a CSD, we obtain the island parity and relative charge occupation for different gate voltages, and thereby infer which charge states hybridize. Both devices are tuned into a TQD by lowering barrier voltages T3 and T4 into weak tunneling regimes. Subsequently, barriers T2 and T5 are set to strongly negative voltages to prevent electrons from tunneling to the leads. In this "floating" regime total charge is conserved, leaving only two charge degrees of freedom. It is therefore sufficient to vary two gate voltages (e.g., V_L and V_R) to reach any available charge state or transition.

To probe the system's charge stability we employ DGS, measuring complex transmission responses A_i for $i \in \{L, M, R\}$ of each of the corresponding top gates' resonators simultaneously with frequency multiplexing. The responses are projected and normalized to produce real-valued quantities A_i' (Supplemental Material [40] Sec. SI), then superimposed in a single CSD to emphasize correlations. The resulting three-dimensional color map and CSDs are shown in Figs. 1(d) and 1(f). We observe white Coulomb-blockaded regions separated by charge transitions where electrons hybridize between QDs. As DGS reflects resonant tunneling, the resonators connected to all involved QDs show a response. For the transition between island M and QDL for example, a response is expected in A_M' and A_L', appearing blue in the CSD. Similarly, the transition between island M and QDR appears red. These transitions are most prominent since they are first-order tunneling processes. Meanwhile, an electron tunneling from QDL to QDR corresponds to a cotunneling transition via island M [42,43]. These transitions appear green, but are much weaker than the first-order transitions in this configuration.

Comparing the CSDs of Fig. 1(f), there is a stark difference between device A and B: the former exhibits rectangular regions of stable charge when the SCI has odd parity, while the latter shows only hexagonal Coulomb-blockaded regions. To understand this difference, we compare with charge-state simulations of the QD system combined with an input-output theory calculation of a representative resonator response, shown in Fig. 1(e) [28,44–46]. For these, we use the inferred values of E_C^S, E_C^N, and E_0, and resonator parameters from Ref. [28]. Extracting the lowest-energy states of the system with a capacitance model allows for calculating a theoretical resonator response [46–48] (Supplemental Material [40] Sec. SIII). States are labeled with the relative number of electrons in dots L, M, and R, respectively, with 0 charge
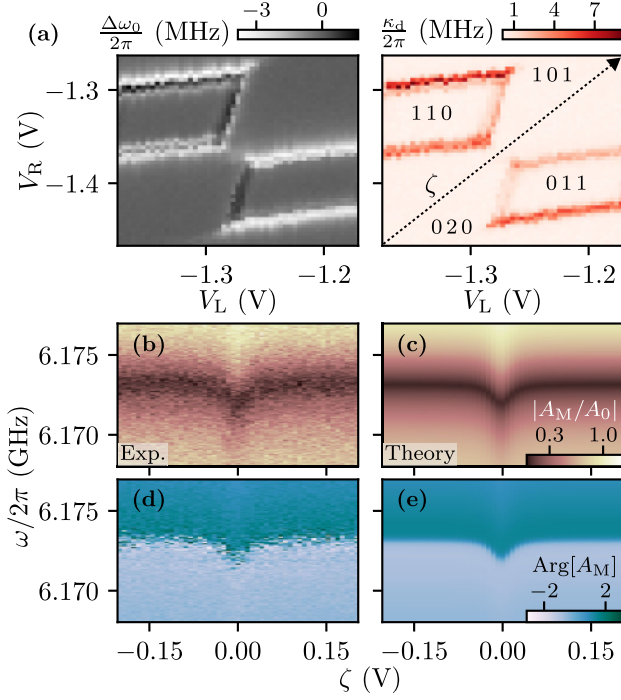
FIG. 2. Middle resonator response in the floating TQD regime of device A. (a) The resonance frequency shift $\Delta\omega_0$ and linewidth κ_d of the middle resonator. (b),(d) Phase and amplitude response of resonator M along the ζ axis defined in (a). (c),(e) Fits of the response to a low-energy CAR model.

on island M corresponding to an even charge. As expected, transitions separating two charge states show response only from resonators coupled to the involved QDs. The different structure between the two CSDs is controlled by the conditions $E_C^S < E_0$ (device A) or $E_C^S > E_0$ (device B). Crucially, in device A, a transition between (0 2 0) and (1 0 1) can be observed, corresponding to a Cooper pair leaving the SCI while QDL and QDR each gain an electron. Conversely, device B only exhibits transitions involving the exchange of single electrons.

Next, we examine this (0 2 0)-(1 0 1) transition—only reachable if $E_C^S < E_0$ as for device A—in more detail in Fig. 2. The frequency response of the island M resonator is measured at each gate voltage then fitted to a complex transmission model [49–51]. In Fig. 2(a), the obtained resonance frequency shifts from the value in Coulomb blockade $\Delta\omega_0$ and photon decay rates κ_d are shown. The resonator responds strongly for single-electron transitions with $\Delta\omega_0 > 2\pi \times 2.5$ MHz.

We isolate the (0 2 0)-(1 0 1) transition by measuring along the arrow labeled ζ, defined as $V_L + V_R$ up to an offset, in Fig. 2(a). This is approximately equivalent to changing island M's gate voltage in the opposite direction. Figures 2(b) and 2(d) show the response across the transition, where a significant dispersive shift $\Delta\omega_0 > 2\pi \times 1$ MHz is observed. There, the underlying tunneling process is likely CPS dominated by coherent CAR [48], since other processes

are suppressed by large energy costs of breaking a Cooper pair $2E_0$ or by E_C^N. Additionally, a lesser cost $E_0 - E_C^S$ suppresses (0 2 0)-(1 0 1) transitions involving intermediate (1 1 0) or (0 1 1) states with a quasiparticle on the SCI. Including single-electron tunnel couplings however, these states may be weakly occupied as the least energetically unfavorable states mediating a CPS process, namely, CAR [2,52]. CAR mediated by the Al shell is suppressed by the length of the SCI, $L = 1.2$ μm over the superconducting coherence length, ξ, as $\exp(-L/\pi\xi)$ [53], but can also be mediated by extended bound states in the proximitized InAs [13,54]. Given a ξ of 260 nm reported in similar nanowires [55], we conclude CAR-dominated CPS is likely.

To corroborate this conclusion, we use a low-energy Hamiltonian describing CAR mediated by an arbitrary number of degenerate quasiparticle states and fit the resonator response to its corresponding input-output model [16,28,43,44,46,56,57] (Supplemental Material [40] Sec. SIV). From the fit, we extract the effective electron- and holelike tunnel couplings $t_{\text{eff},e/h}$ leading to coupling between the (0 2 0) and (1 0 1) states [58]. Resonator parameters are fixed by fits from Fig. 2(a), while the ζ lever arm is estimated from Coulomb diamond measurements. This leaves $t_{\text{eff},e/h}$, the total dephasing and decay rate γ, and the resonator coupling to the (0 2 0)-(1 0 1) transition g_c as free parameters. The fit is plotted in Figs. 2(c) and 2(e), showing excellent agreement with the data for coherent tunneling amplitudes of $t_{\text{eff},h} = t_{\text{eff},e}/1.1 = 2\pi \times 24$ GHz, $\gamma/2\pi$ of 1.1 GHz, and $g_c/2\pi$ of 0.23 GHz. Notably, $t_{\text{eff},e/h}$ is substantially smaller than the $2E_0$ or E_C^N costs of non-CAR-related tunneling processes, and the dephasing rate is more than an order of magnitude smaller than the single-electron tunneling amplitudes. This relation of parameters indicates that the (0 2 0)-(1 0 1) transition corresponds to the coherent splitting of a Cooper pair by crossing a single resonant charge transition.

Future experiments may increase the size in gate space of the CPS transition by increasing E_0/E_C^S, or increase the CAR amplitude by reducing the SCI length relative to ξ. Concurrently, the presence of this transition requires that $E_C^S \leq E_0$, necessitating a large total capacitance of the SCI. These conditions may be simultaneously met using methods presented in Ref. [59] to extend the SCI perpendicular to the nanowire, or to replace it with a grounded superconductor as demonstrated in Ref. [13]. Conversely, a finite E_C^S or ungrounded superconductor protects the SCI from quasiparticle poisoning [60], reducing the probability of independent quasiparticles entering the QDs instead of a split pair.

Having observed a CPS transition in a floating system, we next demonstrate how a split pair's electrons may be detected without external charge sensors in this experimental geometry. In particular, to detect a single charge tunneling into a QD it suffices to measure changes in the

dot's parity, which we show is achievable using a DQD probed with DGS. For an isolated DQD where the total charge is fixed, interdot transitions are spaced in chemical potential by the sum of the dots' charging energies [48]. An electron tunneling into the DQD flips the charge parity and shifts one QD's chemical potential by E_C^N, offsetting these transitions by half their spacing and potentially shifting the system from Coulomb blockade to charge degeneracy or vice versa. It has been shown that blockade and charge degeneracy can be distinguished rapidly with DGS [16–29], hence DGS is sensitive to parity changes in a coupled DQD. Furthermore, the readout signal persists for most interdot detunings $\delta = V_R - V_P$ if the dots are strongly hybridized, illustrated by a sweep of δ in Fig. 3(c). Notably, if the dot orbitals are also spin polarized, Pauli spin blockade renders this sensing principle a spin measurement via spin-to-charge conversion [32,61].

We implement this method in a floating quadruple dot configuration in device B, shown in Fig. 1(b), since the performance of device A deteriorated after multiple thermal cycles. We stress, however, that the parity sensor signal is independent of the origin of electrons flipping its parity and the properties of the coupled SCI. Hence, this technique is equally applicable to devices with a CPS transition or other Coulomb-blockaded systems. In the quadruple dot regime, we aim to observe parity changes in the DQD formed by QDR and QDP. To reach this configuration, T5 is tuned to a strong tunneling regime such that these dots form a DQD while effectively sharing a single charging energy [47]. Additionally, T2 and T6 are pinched-off to prevent tunneling to the leads, effectively removing one charge degree of freedom. We use as voltage coordinates V_L together with the detuning between the rightmost two dots δ and the voltages' average $\epsilon = (V_R + V_L)/2$, both defined up to an offset, see Fig. 3(a).

The data acquisition method for this measurement is identical to the procedure outlined for Fig. 1(f). Here, three-dimensional CSDs are measured: sweeping δ, ϵ, and V_L. Slices are shown in Fig. 3(b) for δ values chosen such that the sensor DQD is on charge degeneracy for even or odd parity. The yellow regions signify that an electron is hybridizing between QDR and a QD whose resonator is unrepresented in the color map [cf. Fig. 3(c)], which is QDP by exclusion. Notably, the charge plateaus for which resonator R responds are opposite between the two δ values, and opposite whenever the sensor changes parity.

Next, we show in Fig. 3(c) the response of resonator P as a function of δ measured at the circle and square markers in Fig. 3(b). We phenomenologically fit the Coulomb oscillations with a periodic Lorentzian and observe that Coulomb resonance for the solid line occurs exactly when the dashed line shows Coulomb blockade. Fixing the peak spacing, we repeat this fitting procedure for all voltages shown in the CSD. Importantly, the detuning offset δ_r of the pattern quantifies the position of charge degeneracy in the
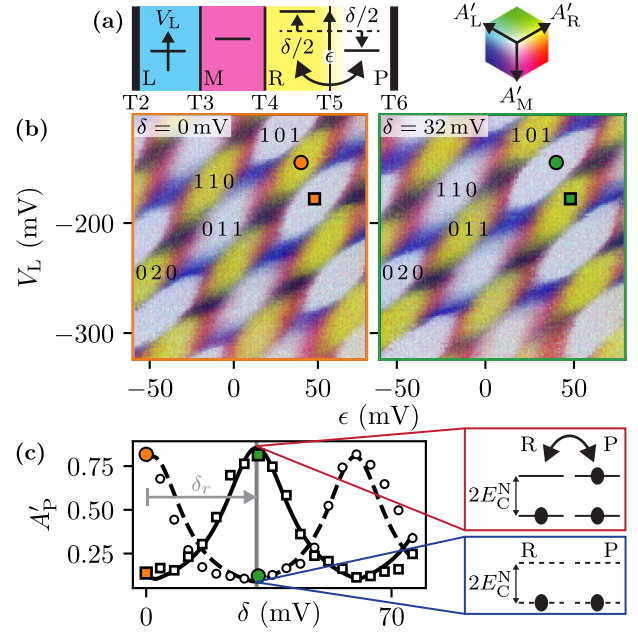

FIG. 3. Parity measurement using a DQD in device B. (a) Chemical potential schematic of the quadruple dot. (b) Multiplexed CSDs in the floating quadruple dot regime at fixed $\delta = 0$ mV on the left and 32 mV on the right, with the color map shown above. Charge plateaus are labeled to represent the relative occupancy of the dots where the rightmost number represents the combined occupation of QDR and QDP. The individual resonator responses are shown in Supplemental Material [40] Sec. SI. (c) Linecuts of the resonator P response as a function of δ, measured at voltages indicated by the square and circle markers in (b). The solid and dashed curves show fits to a periodic Lorentzian. At zero detuning between the dots, resonator P shows a response for one parity value, but is blockaded for the other. The insets show cartoons of the sensor DQD levels in both cases.

window -14 mV $< \delta < 43$ mV, allowing inference of the DQD's relative parity.

To demonstrate this correspondence, we plot δ_r in Fig. 4. Clear regions corresponding to the two sensor DQD parities are visible, consistent with the histogram of δ_r values shown on the right. The stark splitting of δ_r values demonstrates that readout of parity changes can be accomplished by fixing δ to a value maximizing contrast, such as $\delta = 0$ in this case. This may be extended to single-shot readout provided electrons reside on the sensor DQD longer than the readout time. Placing one DQD sensor on either side of a superconducting reservoir or island would then enable time-resolved detection of both electrons from a split Cooper pair.

We have realized a normal-superconducting-normal hybrid QD system in an InAs nanowire. Multiplexed DGS shows different resonators responding depending on the spatial distribution of tunneling electrons, enabling us to infer the QDs' relative charge states [28,38]. With DGS we observe a coherent CPS transition, repelling two electrons from the SCI to the surrounding QDs. Crossing this transition splits a single Cooper pair controllably and
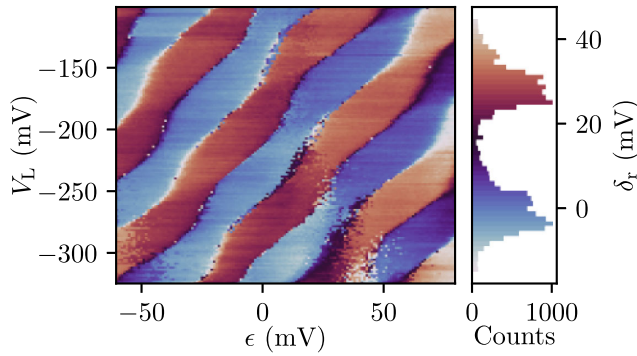
FIG. 4. Distinguishment of parity in the floating quadruple dot regime for device B. The detuning for which the sensor DQD is on resonance, -14 mV $< \delta_r < 43$ mV, is shown. On the right, a histogram of δ_r value occurrences defines the color map of the stability diagram.

retains the resulting individual electrons on the outer dots. Importantly, this transition cannot occur concurrently to interdot cotunneling except for the fine-tuned parameters $E_C^S = E_0$ in a floating TQD, constraining applications to quasiparticle-poisoning-protected Kitaev chains [62–64]. Furthermore, we have shown that DGS of a DQD is sensitive to its parity and can be used to detect electrons ejected from a neighboring SCI. Lastly, we note the demonstrated sensing method becomes a spin measurement of electrons entering the DQD when its levels are spin-polarized [21–24,27,61]. Two such detectors on either side of a superconductor, combined with spin manipulation techniques [65–69], would enable performing a Bell test verifying the spin-singlet entanglement of electrons in Cooper pairs [32–36]. This is possible through comparison with the Clauser-Horne-Shimony-Holt inequality for the two spin qubits formed by the detectors, initialized to entangled states by pulsing gate voltages across the CPS transition [70,71].

Raw data, analysis code, and scripts for plotting the figures in this Letter are available from Zenodo [72].

*Corresponding author: cprosko@ualberta.net

[1] G. Lesovik, T. Martin, and G. Blatter, Electronic entanglement in the vicinity of a superconductor, Eur. Phys. J. B **24**, 287 (2001).

[2] P. Recher, E. V. Sukhorukov, and D. Loss, Andreev tunneling, Coulomb blockade, and resonant transport of nonlocal spin-entangled electrons, Phys. Rev. B **63**, 165314 (2001).

[3] L. Hofstetter, S. Csonka, J. Nygård, and C. Schönenberger, Cooper pair splitter realized in a two-quantum-dot Y-junction, Nature (London) **461**, 960 (2009).

[4] L. G. Herrmann, F. Portier, P. Roche, A. L. Yeyati, T. Kontos, and C. Strunk, Carbon Nanotubes as Cooper-Pair Beam Splitters, Phys. Rev. Lett. **104**, 026801 (2010).

[5] A. Das, Y. Ronen, M. Heiblum, D. Mahalu, A. V. Kretinin, and H. Shtrikman, High-efficiency Cooper pair splitting demonstrated by two-particle conductance resonance and positive noise cross-correlation, Nat. Commun. **3**, 1165 (2012).

[6] J. Schindele, A. Baumgartner, and C. Schönenberger, Near-Unity Cooper Pair Splitting Efficiency, Phys. Rev. Lett. **109**, 157002 (2012).

[7] Z. B. Tan, D. Cox, T. Nieminen, P. Lähteenmäki, D. Golubev, G. B. Lesovik, and P. J. Hakonen, Cooper Pair Splitting by Means of Graphene Quantum Dots, Phys. Rev. Lett. **114**, 096602 (2015).

[8] R. S. Deacon, A. Oiwa, J. Sailer, S. Baba, Y. Kanai, K. Shibata, K. Hirakawa, and S. Tarucha, Cooper pair splitting in parallel quantum dot Josephson junctions, Nat. Commun. **6**, 7446 (2015).

[9] I. V. Borzenets, Y. Shimazaki, G. F. Jones, M. F. Craciun, S. Russo, M. Yamamoto, and S. Tarucha, High efficiency CVD graphene-lead (Pb) Cooper pair splitter, Sci. Rep. **6**, 23051 (2016).

[10] S. Baba, C. Jünger, S. Matsuo, A. Baumgartner, Y. Sato, H. Kamata, K. Li, S. Jeppesen, L. Samuelson, H. Q. Xu, C. Schönenberger, and S. Tarucha, Cooper-pair splitting in two parallel InAs nanowires, New J. Phys. **20**, 063021 (2018).

[11] P. Pandey, R. Danneau, and D. Beckmann, Ballistic Graphene Cooper Pair Splitter, Phys. Rev. Lett. **126**, 147701 (2021).

[12] O. Kürtössy, Z. Scherübl, G. Fülöp, I. E. Lukács, T. Kanne, J. Nygård, P. Makk, and S. Csonka, Parallel InAs nanowires for Cooper pair splitters with Coulomb repulsion, npj Quantum Mater. **7**, 88 (2022).

[13] G. Wang, T. Dvir, G. P. Mazur, C.-X. Liu, N. van Loo, S. L. D. ten Haaf, A. Bordin, S. Gazibegovic, G. Badawy, E. P. A. M. Bakkers, M. Wimmer, and L. P. Kouwenhoven, Singlet and triplet Cooper pair splitting in hybrid superconducting nanowires, Nature (London) **612**, 448 (2022).

[14] A. Bordoloi, V. Zannier, L. Sorba, C. Schönenberger, and A. Baumgartner, Spin cross-correlation experiments in an electron entangler, Nature (London) **612**, 454 (2022).

[15] A. Ranni, F. Brange, E. T. Mannila, C. Flindt, and V. F. Maisi, Real-time observation of Cooper pair splitting showing strong non-local correlations, Nat. Commun. **12**, 6358 (2021).

[16] K. D. Petersson, C. G. Smith, D. Anderson, P. Atkinson, G. A. C. Jones, and D. A. Ritchie, Charge and spin state readout of a double quantum dot coupled to a resonator, Nano Lett. **10**, 2789 (2010).

[17] T. Frey, P. J. Leek, M. Beck, A. Blais, T. Ihn, K. Ensslin, and A. Wallraff, Dipole Coupling of a Double Quantum Dot to a Microwave Resonator, Phys. Rev. Lett. **108**, 046807 (2012).

[18] J. I. Colless, A. C. Mahoney, J. M. Hornibrook, A. C. Doherty, H. Lu, A. C. Gossard, and D. J. Reilly, Dispersive Readout of a Few-Electron Double Quantum Dot with Fast rf Gate Sensors, Phys. Rev. Lett. **110,** 046805 (2013).

[19] A. C. Betz, R. Wacquez, M. Vinet, X. Jehl, A. L. Saraiva, M. Sanquer, A. J. Ferguson, and M. F. Gonzalez-Zalba, Dispersively detected Pauli spin-blockade in a silicon nanowire field-effect transistor, Nano Lett. **15,** 4622 (2015).

[20] N. J. Lambert, A. A. Esmail, M. Edwards, F. A. Pollock, B. W. Lovett, and A. J. Ferguson, Quantum capacitance and charge sensing of a superconducting double dot, Appl. Phys. Lett. **109,** 112603 (2016).

[21] P. Pakkiam, A. V. Timofeev, M. G. House, M. R. Hogg, T. Kobayashi, M. Koch, S. Rogge, and M. Y. Simmons, Single-Shot Single-Gate rf Spin Readout in Silicon, Phys. Rev. X **8,** 041032 (2018).

[22] M. Urdampilleta, D. J. Niegemann, E. Chanrion, B. Jadot, C. Spence, P.-A. Mortemousque, C. Bäuerle, L. Hutin, B. Bertrand, S. Barraud, R. Maurand, M. Sanquer, X. Jehl, S. D. Franceschi, M. Vinet, and T. Meunier, Gate-based high fidelity spin readout in a CMOS device, Nat. Nanotechnol. **14,** 737 (2019).

[23] A. West, B. Hensen, A. Jouan, T. Tanttu, C.-H. Yang, A. Rossi, M. F. Gonzalez-Zalba, F. Hudson, A. Morello, D. J. Reilly, and A. S. Dzurak, Gate-based single-shot readout of spins in silicon, Nat. Nanotechnol. **14,** 437 (2019).

[24] G. Zheng, N. Samkharadze, M. L. Noordam, N. Kalhor, D. Brousse, A. Sammak, G. Scappucci, and L. M. K. Vandersypen, Rapid gate-based spin read-out in silicon using an on-chip resonator, Nat. Nanotechnol. **14,** 742 (2019).

[25] D. de Jong, J. van Veen, L. Binci, A. Singh, P. Krogstrup, L. P. Kouwenhoven, W. Pfaff, and J. D. Watson, Rapid Detection of Coherent Tunneling in an InAs Nanowire Quantum Dot through Dispersive Gate Sensing, Phys. Rev. Appl. **11,** 044061 (2019).

[26] D. Sabonis, E. C. T. O'Farrell, D. Razmadze, D. M. T. van Zanten, J. Suter, P. Krogstrup, and C. M. Marcus, Dispersive sensing in hybrid InAs/Al nanowires, Appl. Phys. Lett. **115,** 102601 (2019).

[27] A. Crippa, R. Ezzouch, A. Aprá, A. Amisse, R. Laviéville, L. Hutin, B. Bertrand, M. Vinet, M. Urdampilleta, T. Meunier, M. Sanquer, X. Jehl, R. Maurand, and S. D. Franceschi, Gate-reflectometry dispersive readout and coherent control of a spin qubit in silicon, Nat. Commun. **10,** 2776 (2019).

[28] D. de Jong, C. G. Prosko, D. M. A. Waardenburg, L. Han, F. K. Malinowski, P. Krogstrup, L. P. Kouwenhoven, J. V. Koski, and W. Pfaff, Rapid Microwave-Only Characterization and Readout of Quantum Dots Using Multiplexed Gigahertz-Frequency Resonators, Phys. Rev. Appl. **16,** 014007 (2021).

[29] D. J. Ibberson, T. Lundberg, J. A. Haigh, L. Hutin, B. Bertrand, S. Barraud, C.-M. Lee, N. A. Stelmashenko, G. A. Oakes, L. Cochrane, J. W. A. Robinson, M. Vinet, M. F. Gonzalez-Zalba, and L. A. Ibberson, Large dispersive interaction between a CMOS double quantum dot and microwave photons, PRX Quantum **2,** 020315 (2021).

[30] L. Han, M. Chan, D. de Jong, C. Prosko, G. Badawy, S. Gazibegovic, E. P. A. M. Bakkers, L. P. Kouwenhoven, F. K. Malinowski, and W. Pfaff, Variable and Orbital-Dependent Spin-Orbit Field Orientations in an InSb Double Quantum Dot Characterized via Dispersive Gate Sensing, Phys. Rev. Appl. **19,** 014063 (2023).

[31] R. Hanson, L. P. Kouwenhoven, J. R. Petta, S. Tarucha, and L. M. K. Vandersypen, Spins in few-electron quantum dots, Rev. Mod. Phys. **79,** 1217 (2007).

[32] Z. Scherübl, A. Pályi, and S. Csonka, Probing individual split Cooper pairs using the spin qubit toolkit, Phys. Rev. B **89,** 205439 (2014).

[33] A. Einstein, B. Podolsky, and N. Rosen, Can quantum-mechanical description of physical reality be considered complete?, Phys. Rev. **47,** 777 (1935).

[34] J. S. Bell, On the Einstein Podolsky Rosen paradox, Phys. Phys. Fiz. **1,** 195 (1964).

[35] N. M. Chtchelkatchev, G. Blatter, G. B. Lesovik, and T. Martin, Bell inequalities and entanglement in solid-state devices, Phys. Rev. B **66,** 161320(R) (2002).

[36] P. Samuelsson, E. V. Sukhorukov, and M. Büttiker, Orbital Entanglement and Violation of Bell Inequalities in Mesoscopic Conductors, Phys. Rev. Lett. **91,** 157002 (2003).

[37] J. G. Kroll, F. Borsoi, K. L. van der Enden, W. Uilhoorn, D. de Jong, M. Quintero-Pérez, D. J. van Woerkom, A. Bruno, S. R. Plissard, D. Car, E. P. A. M. Bakkers, M. C. Cassidy, and L. P. Kouwenhoven, Magnetic-Field-Resilient Superconducting Coplanar-Waveguide Resonators for Hybrid Circuit Quantum Electrodynamics Experiments, Phys. Rev. Appl. **11,** 064053 (2019).

[38] A. Ruffino, T.-Y. Yang, J. Michniewicz, Y. Peng, E. Charbon, and M. F. Gonzalez-Zalba, A cryo-CMOS chip that integrates silicon quantum dots and multiplexed dispersive readout electronics, National electronics review **5,** 53 (2021).

[39] J. M. Hornibrook, J. I. Colless, A. C. Mahoney, X. G. Croot, S. Blanvillain, H. Lu, A. C. Gossard, and D. J. Reilly, Frequency multiplexing for readout of spin qubits, Appl. Phys. Lett. **104,** 103108 (2014).

[40] See Supplemental Material at http://link.aps.org/supplemental/10.1103/PhysRevLett.131.157001 for details of signal processing, theoretical modeling, fits of the data, and measurements of device properties.

[41] C. Macklin, K. O'Brien, D. Hover, M. E. Schwartz, V. Bolkhovsky, X. Zhang, W. D. Oliver, and I. Siddiqi, A near-quantum-limited Josephson traveling-wave parametric amplifier, Science **350,** 307 (2015).

[42] D. V. Averin and Y. V. Nazarov, Macroscopic quantum tunneling of charge and co-tunneling, in *Single Charge Tunneling: Coulomb Blockade Phenomena in Nanostructures*, edited by H. Grabert and M. H. Devoret (Plenum Press and NATO Scientific Affairs Division, New York/London, 1992), pp. 217–247.

[43] F. R. Braakman, P. Barthelemy, C. Reichl, W. Wegscheider, and L. M. K. Vandersypen, Long-distance coherent coupling in a quantum dot array, Nat. Nanotechnol. **8,** 432 (2013).

[44] M. J. Collett and C. W. Gardiner, Squeezing of intracavity and traveling-wave light fields produced in parametric amplification, Phys. Rev. A **30,** 1386 (1984).

[45] G. Burkard and J. R. Petta, Dispersive readout of valley splittings in cavity-coupled silicon quantum dots, Phys. Rev. B **94,** 195305 (2016).

[46] J. V. Koski, A. J. Landig, M. Russ, J. C. Abadillo-Uriel, P. Scarlino, B. Kratochwil, C. Reichl, W. Wegscheider, G. Burkard, M. Friesen, S. N. Coppersmith, A. Wallraff, K. Ensslin, and T. Ihn, Strong photon coupling to the quadrupole moment of an electron in a solid-state qubit, Nat. Phys. **16**, 642 (2020).

[47] W. G. van der Wiel, S. De Franceschi, J. M. Elzerman, T. Fujisawa, S. Tarucha, and L. P. Kouwenhoven, Electron transport through double quantum dots, Rev. Mod. Phys. **75**, 1 (2002).

[48] J. van Veen, D. de Jong, L. Han, C. Prosko, P. Krogstrup, J. D. Watson, L. P. Kouwenhoven, and W. Pfaff, Revealing charge-tunneling processes between a quantum dot and a superconducting island through gate sensing, Phys. Rev. B **100**, 174508 (2019).

[49] M. S. Khalil, M. J. A. Stoutimore, F. C. Wellstood, and K. D. Osborn, An analysis method for asymmetric resonator transmission applied to superconducting devices, J. Appl. Phys. **111**, 054510 (2012).

[50] S. Probst, F. B. Song, P. A. Bushev, A. V. Ustinov, and M. Weides, Efficient and robust analysis of complex scattering data under noise in microwave resonators, Rev. Sci. Instrum. **86**, 024706 (2015).

[51] H. Guan, M. Dai, Q. He, J. Hu, P. Ouyang, Y. Wang, L. F. Wei, and J. Gao, Network modeling of non-ideal superconducting resonator circuits, Supercond. Sci. Technol. **33**, 075004 (2020).

[52] L. E. Bruhat, T. Cubaynes, J. J. Viennot, M. C. Dartiailh, M. M. Desjardins, A. Cottet, and T. Kontos, Circuit QED with a quantum-dot charge qubit dressed by Cooper pairs, Phys. Rev. B **98**, 155313 (2018).

[53] M. Leijnse and K. Flensberg, Coupling Spin Qubits via Superconductors, Phys. Rev. Lett. **111**, 060501 (2013).

[54] C.-X. Liu, G. Wang, T. Dvir, and M. Wimmer, Tunable Superconducting Coupling of Quantum Dots via Andreev Bound States in Semiconductor-Superconductor Nanowires, Phys. Rev. Lett. **129**, 267701 (2022).

[55] S. M. Albrecht, A. P. Higginbotham, M. Madsen, F. Kuemmeth, T. S. Jespersen, J. Nygård, P. Krogstrup, and C. M. Marcus, Exponential protection of zero modes in Majorana islands, Nature (London) **531**, 206 (2016).

[56] J. R. Schrieffer and P. A. Wolff, Relation between the Anderson and Kondo Hamiltonians, Phys. Rev. **149**, 491 (1966).

[57] J. Eldridge, M. G. Pala, M. Governale, and J. König, Superconducting proximity effect in interacting double-dot systems, Phys. Rev. B **82**, 184507 (2010).

[58] Esben Bork Hansen, Jeroen Danon, and Karsten Flensberg, Probing electron-hole components of subgap states in Coulomb blockaded Majorana islands, Phys. Rev. B **97**, 041411 (2018).

[59] S. Heedt, M. Quintero-Pérez, F. Borsoi, A. Fursina, N. van Loo, G. P. Mazur, M. P. Nowak, M. Ammerlaan, K. Li, S. Korneychuk, J. Shen, M. A. Y. van de Poll, G. Badawy, S. Gazibegovic, N. de Jong, P. Aseev, K. van Hoogdalem, E. P. A. M. Bakkers, and L. P. Kouwenhoven, Shadow-wall lithography of ballistic superconductor–semiconductor quantum devices, Nat. Commun. **12**, 4914 (2021).

[60] H. Q. Nguyen, D. Sabonis, D. Razmadze, E. T. Mannila, V. F. Maisi, D. M. T. van Zanten, E. C. T. O'Farrell, P. Krogstrup, F. Kuemmeth, J. P. Pekola, and C. M. Marcus, Electrostatic control of quasiparticle poisoning in a hybrid semiconductor-superconductor island, Phys. Rev. B **108**, L041302 (2023).

[61] A. Cottet, C. Mora, and T. Kontos, Mesoscopic admittance of a double quantum dot, Phys. Rev. B **83**, 121311(R) (2011).

[62] T. Dvir, G. Wang, N. van Loo, C.-X. Liu, G. P. Mazur, A. Bordin, S. L. D. ten Haaf, J.-Y. Wang, D. van Driel, F. Zatelli, X. Li, F. K. Malinowski, S. Gazibegovic, G. Badawy, E. P. A. M. Bakkers, M. Wimmer, and L. P. Kouwenhoven, Realization of a minimal Kitaev chain in coupled quantum dots, Nature (London) **614**, 445 (2023).

[63] T. Karzig, C. Knapp, R. M. Lutchyn, P. Bonderson, M. B. Hastings, C. Nayak, J. Alicea, K. Flensberg, S. Plugge, Y. Oreg, C. M. Marcus, and M. H. Freedman, Scalable designs for quasiparticle-poisoning-protected topological quantum computation with Majorana zero modes, Phys. Rev. B **95**, 235305 (2017).

[64] S. Plugge, A. Rasmussen, R. Egger, and K. Flensberg, Majorana box qubits, New J. Phys. **19**, 012001 (2017).

[65] V. N. Golovach, M. Borhani, and D. Loss, Electric-dipole-induced spin resonance in quantum dots, Phys. Rev. B **74**, 165319 (2006).

[66] C. Flindt, A. S. Sørensen, and K. Flensberg, Spin-Orbit Mediated Control of Spin Qubits, Phys. Rev. Lett. **97**, 240501 (2006).

[67] K. C. Nowack, F. H. L. Koppens, Y. V. Nazarov, and L. M. K. Vandersypen, Coherent control of a single electron spin with electric fields, Science **318**, 1430 (2007).

[68] S. Nadj-Perge, S. M. Frolov, E. P. A. M. Bakkers, and L. P. Kouwenhoven, Spin–orbit qubit in a semiconductor nanowire, Nature (London) **468**, 1084 (2010).

[69] M. D. Schroer, K. D. Petersson, M. Jung, and J. R. Petta, Field Tuning the g Factor in InAs Nanowire Double Quantum Dots, Phys. Rev. Lett. **107**, 176811 (2011).

[70] J. P. Dehollain, S. Simmons, J. T. Muhonen, R. Kalra, A. Laucht, F. Hudson, K. M. Itoh, D. N. Jamieson, J. C. McCallum, A. S. Dzurak, and A. Morello, Bell's inequality violation with spins in silicon, Nat. Nanotechnol. **11**, 242 (2016).

[71] John F. Clauser, Michael A. Horne, Abner Shimony, and Richard A. Holt, Proposed Experiment to Test Local Hidden Variable Theories, Phys. Rev. Lett. **24**, 549 (1970).

[72] D. de Jong, C. G. Prosko, L. Han, F. K. Malinowski, Y. Liu, L. P. Kouwenhoven, and W. Pfaff, Data repository accompanying, "Controllable single Cooper pair splitting in hybrid quantum dot systems", 10.5281/zenodo.7842384.